Nanospray Dielectrophoresis

Marcel Tichem and Richard R. A. Syms, *Senior Member, IEEE*

***Abstract*—Self-assembly of nanoparticles into microscale patterns by spray deposition and dielectrophoresis is investigated using microfabricated RF traps and nanospheres visualized using confocal fluorescence microscopy. Different combinations of spraying mode and trapping field lead to different results. Pneumatic spray and dielectrophoresis leads to sharply defined patterns at electrode edges, at the expense of particle clustering. In contrast, nanospray dielectrophoresis leads to improved particle dispersion due to charge repulsion, but suffers from dc focusing effects due to surface charges. Controlled switching between the different modes is demonstrated by manipulating the charge state of the nanospheres and the trapping potential.**

***Index Terms*—Dielectrophoresis (DEP), nanospray, pneumatic spray, self-assembly, trapping.**

I. Introduction

NANOPARTICLES such as carbon nanotubes (CNTs) and nanowires have unique properties with the potential to allow new materials, devices, and functions. However, volume production processes are required for integration into device formats. In bulk applications, nanoparticles are distributed over a volume, as fillers to enhance material properties. Specified orientations may be used to obtain anisotropy. Patterned arrangements vary from individual particles at discrete locations (e.g., in nanoprobes) to large numbers of particles in discrete patterns (in FETs with nanowire channels). In monolithic approaches, the nanoparticles are grown or fabricated *in situ* but this approach places significant demands on process compatibility. In heterogeneous assembly methods, they are prefabricated and guided into the desired arrangement. This approach offers more freedom in processing, at the cost of increased patterning effort.

There are three main approaches to heterogeneous assembly: discrete robot-based manipulation, (bio-)chemical templates, and force fields. In the first, handling is simply scaled down to the nanolevel, for example, using microrobots working under an optical or scanning electron microscope [1]. Although this approach allows single object patterns to be created, it suffers from difficulties in observation and handling, and an inherent lack of scalability. The second involves chemical templates and can easily create large-scale nanopatterns. Techniques such as dip pen nanolithography and microcontact printing are used to create local patterns of self-assembled monolayers, controlling the surface wettability and providing chemical groups for binding [2]. Binding forces can be specific and strong, and self-assembly allows for massive parallelism. However, this approach requires additional chemical functionalization and a fluidic environment.

In the third approach, objects are trapped and aligned by a force field. Many physical forces have now been explored. Viscous forces have been used to align 1-D nanostructures in a gas flow [3]. Close-packed arrays have been created by convective self-assembly in liquid [4]. This process can be further controlled using lithographically defined features, variations in wettability, and chemical functionalization [5]. Optical trapping [6], [7] and magnetic fields [8] have also been proposed for handling nanowires and nanotubes in suspension. In electrostatic patterning, charged objects are trapped by a dc potential. Trapping can be from both liquid and gas phases, while electrodes may be realized by writing with a conductive atomic force microscope tip (in nanoxerography) [9], charge patterns or electrode patterns [10], [11].

In dielectrophoresis (DEP), dielectric particles form dipoles that are subject to a net force in an inhomogeneous electric field [12]. Smith *et al.* [13] were among the first to produce lithographically defined electrodes to align nanowires from suspension. Since then, wires [14] and CNTs [15] have been successfully trapped. DC DEP has also been demonstrated for concentrating and trapping nanoparticles and nanowires [16], [17]. Since the particles are polarized during DEP, they may have an additional tendency to chain, and this feature has been exploited for wire formation [18], [19]. AC DEP offers considerably more freedom than either Coulomb forces or dc DEP. The force is in both sign and magnitude a function of the particle size and orientation, its dielectric properties, and the frequency and strength of the applied field, allowing considerable potential for separation and sorting [20], [21].

In all the examples above, the nanoparticles were scavenged from solution. In this case, viscous forces are strong, since they scale with the first order of object size whereas the trapping forces scale with the second or third order. Scavenging from the gas phase in a directed spray has several advantages: a significant reduction in viscous force, and a consequent increase in trapping speed, the ability to direct the spray, and the yield of a dry product. Electrospray has of course been used for deposition of a wide variety of nanoparticles [22], [23]. However, spray-based patterning has received limited attention. Direct writing

Manuscript received June 4, 2012; revised August 7, 2012; accepted September 23, 2012. Date of publication October 9, 2012; date of current version November 16, 2012. This work was supported by a Marie Curie Intra European Fellowship within the Seventh European Community Framework Programme, under Grant 253731, "Discrete Volume Assembly at Nanoscale (DIVAN)." The review of this paper was arranged by Associate Editor J. Li.

M. Tichem was with the Optical and Semiconductor Devices Group, Department of Electrical and Electronic Engineering, Imperial College, London, London, SW7 2BT, U.K., on leave from the Micro and Nano Engineering Laboratory, Delft University of Technology, 2628CD Delft, The Netherlands (e-mail: m.tichem@tudelft.nl).

R. R. A. Syms is with the Optical and Semiconductor Devices Group, Department of Electrical and Electronic Engineering, Imperial College, London, London, SW7 2BT, U.K. (e-mail: r.syms@ic.ac.uk).

Color versions of one or more of the figures in this paper are available online at http://ieeexplore.ieee.org.

Digital Object Identifier 10.1109/TNANO.2012.2223230

has been carried out by substrate translation [24], and stencil patterning has been achieved using apertures [25] and attractive dc forces [26].

In this paper, we provide a systematic investigation of gas-phase trapping, focusing on the effect of dc charge in different ac trapping scenarios by comparing the different combinations of pneumatic and electrospray with DEP for the patterned deposition of fluorescent nanospheres from a suspension. We show that there is inherent competition between the effects of viscous drag, Coulomb force, and both dc and ac dielectrophoretic forces. Section II introduces the concepts involved. Section III provides the theoretical underpinning, while Section IV presents simulation results of the most successful trap type investigated, a microfabricated microstrip. Section V describes the experimental method and results achieved. Controlled manipulation of the trapping mode is demonstrated. Section VI presents conclusions.

II. Spraying and Trapping Modes

We have explored two methods for spray generation: pneumatic spray and electrospray. In pneumatic spray, droplets formed at the end of a narrow capillary are atomized by a coaxial gas flow. The gas promotes solvent evaporation, leaving suspended nanoparticles to be transported by viscous drag, together with residual solvent droplets. The spray humidity is a function of the distance from the spray origin, but can be reduced by heating the gas. Since the particles are uncharged, they will be forced together by surface tension during evaporation. However, large dielectric clusters may easily be trapped using both dc and ac DEP forces.

In electrospray, a coaxial nebulizer is again used. However, the spray is primarily generated using a dc field from a voltage V_D (typically, several kilovolts) applied between the solution and a nearby electrode. Three phases can be distinguished: formation of a Taylor cone from the meniscus at the capillary tip, extrusion of a jet, and separation of the jet into a plume due to Coulomb repulsion [27]. Solvent evaporation again takes place in the plume, leaving a mixture of ions in the flow. One relatively recent development is nanospray, which uses a small-diameter (10–50 μm ID) capillary to reduce the voltage to around 1 kV, without a significant reduction in the ion density [28]. Nanoparticles may also be carried in a spray. Since they are now charged, electrostatic repulsion allows a much finer dispersion, but leads to other effects that complicate trapping.

Trapping is achieved by placing electrodes provided with appropriate ac and dc potentials in the spray path. Fig. 1 shows example geometries that may easily be microfabricated, together with sketches of their equipotentials on a 2-D plane. The simplest is a pair of coplanar electrodes on an insulating layer, as shown in Fig. 1(a). In this case, the electric field forms two concentrations, one at each electrode tip, which provides two DEP trapping foci. Fig. 1(b) shows an alternative arrangement consisting of a conducting strip above a ground plane. For a dielectric interlayer with a relative permittivity close to unity, this arrangement is equivalent to a conducting strip spaced at approximately twice the distance from a second virtual strip

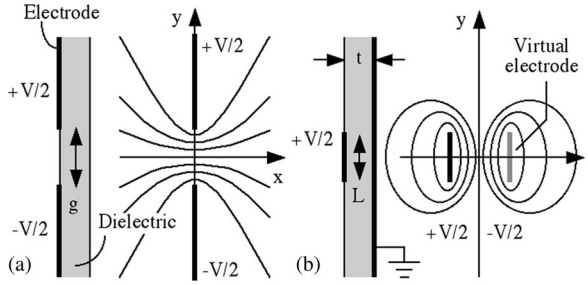

Fig. 1. Geometries for microfabricated traps and sketches of their associated equipotentials: (a) coplanar and (b) microstrip.

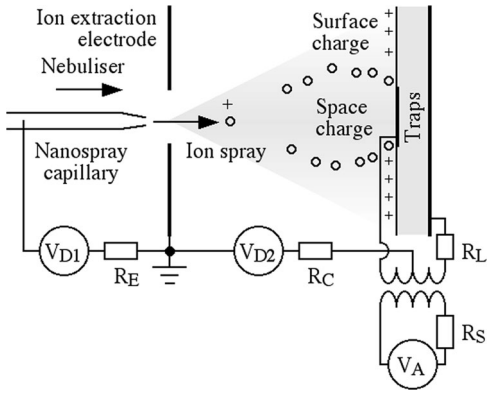

Fig. 2. Arrangement for nanoelectrospray-DEP.

electrode. In this case, four DEP foci are formed, one at each electrode edge; however, only the real foci are important. This configuration has the advantage of reduced sensitivity to dielectric breakdown, especially in a humid spray, because breakdown of the solid interlayer is required for any significant current to flow. Consequently, much of the remainder of this paper is focused on this geometry. However, exposed dielectric may alter behavior if the nanospheres are charged.

Each configuration may be used with either pneumatic or electrospray sources, with an ac potential applied using a signal generator via a step-up transformer. However, for electrospray, dc potentials must also be controlled. Fig. 2 shows an example arrangement for a microstrip trap, in which voltages V_{D1} and V_{D2} are used to generate the spray and apply a bias to the trap, respectively. The voltage dropped across resistors R_E and R_C can be used to monitor ion emission and ion collection. Even with such control, competing effects of trapping and charge repulsion are likely.

III. Theoretical Model

Dielectrophoretic scavenging of neutral particles from a gas flow is subject to a combination of physical effects: inertial and gravitational forces, drag forces due to the gas, and DEP forces in the trapping area. Inertial and gravitational forces can be ignored at the nanosize scale. The drag force is responsible for transportation, and the particles will typically be carried toward and along the trapping surface. When particles are sufficiently close to a trap and moving slowly enough, they will be guided toward it by the dielectrophoretic force, which may be both dc or

ac. Closely separated particles that are uncharged but polarized may also form pearl chains.

In nanospray-DEP, there will be additional Coulomb forces. For example, there will be a space charge within the plume, which is likely to prevent chain formation. The charges of any ions landing on the trapping electrodes may be conducted away. However, microfabricated traps will typically be fabricated on a dielectric, which will charge and then generate a repulsive force for subsequent ions. Surface charging will, therefore, continue only until equilibrium preventing further accumulation is achieved. Nonuniform flux will then give rise to DC DEP even if no DC voltage is present. Finally, if charged particles are sufficiently close to a substrate, image fields will be generated, resulting in additional attractive forces. However, these are short-range.

Solution of problems involving multiple charged particles is notoriously difficult, since Poisson's equation must be satisfied. Although space-charge-dominated solutions have been found for electrospray sources [29], these effects are ignored in simpler models. If equilibrium surface charges are in addition described by a fixed surface potential, the result is an independent-particle model, in which trajectories are determined by solution of Newton's equation for drag, DEP, and electrostatic forces. The first can be determined using the flow of an ideal fluid, while the second and third can be found by solving the simpler Laplace equation. Complexity is further reduced by restriction to two dimensions. Here, we adopt this simplified approach. In this case, the equation of motion of an independent particle (assumed spherical) is

$$\underline{F}_D + \underline{F}_S + \underline{F}_{\rm DC} + \underline{F}_{\rm AC} = 0. \tag{1}$$

Here, $\underline{F}_D$ is the viscous drag force, given by Stokes' law:

$$\underline{F}_D = -6\pi\eta R(\underline{u} - \underline{u}_M). \tag{2}$$

Here, $\underline{u}$ is the particle velocity, $\underline{u}_M$ is the velocity of the background medium, R is the particle radius, and η is the viscosity. The background flow may be modeled by assuming that the gas is an ideal fluid. In this case, for a flow impinging from the –ve x-direction, the velocity distribution $\underline{u}_M$ on the (x, y) plane can be determined from the stream function ψ_M, using the relations $u_{Mx} = -\partial\psi_M/\partial y$ and $u_{My} = \partial\psi_M/\partial x$. For irrotational flow, the stream function satisfies Laplace's equation $\nabla^2\psi_M = 0$ and contours of constant ψ_M are streamlines. For a flow impinging normally on a plate perpendicular to the x-axis, the boundary conditions are $u_{Mx} = 0$ on $x = 0$ (the plate), and $u_{My} = 0$ for large, negative x and small y. A suitable stream function is $\psi_M = Axy$, where A is a constant, giving $u_{Mx} = -Ax$ and $u_{My} = +Ay$.

Similarly, $\underline{F}_S$ is the electrostatic force, given by

$$\underline{F}_S = q\underline{E}_S. \tag{3}$$

Here, $\underline{E}_S$ is the static electric field and q is the charge on the particle. The static field is determined as $\underline{E} = -\nabla\phi_S$, where ϕ_S is the solution of Laplace's equation $\nabla^2\phi_S = 0$ for a system of fixed electrode potentials. Some solutions to (3) are known analytically for thin, unsupported electrodes (for example, the geometry of Fig. 1(a), in the absence of the dielectric). However, since it is difficult to model thick electrodes and dielectric substrates, Laplace's equation must generally be solved numerically (for example, by over-relaxation).

The DEP force has two components: a dc component $\underline{F}_{\rm DC}$ resulting from any time-independent field nonuniformity and an ac component $\underline{F}_{\rm AC}$ resulting from time-varying inhomogeneous fields. Both components can be described by the same expression (again, for a spherical particle):

$$\underline{F} = 2\pi R^3\varepsilon_M\,{\rm Re}[f_{\rm CM}(\omega)]\nabla|\underline{E}|^2. \tag{4}$$

Here, $\underline{E}$ is the electric field, taken as either $\underline{E}_S$ (for static fields) or $\underline{E}_{\rm rms}$ (for ac fields). Similarly, $f_{\rm CM}(\omega)$ is the Clausius–Mossotti factor, to be evaluated at dc for a static field and a specific angular frequency ω for an ac field, and is given by

$$f_{\rm CM} = (\varepsilon_S - {\rm E}_M)/(\varepsilon_S + 2\varepsilon_M). \tag{5}$$

Here, $\varepsilon_S = \varepsilon'_S - j\varepsilon''_S$ and $\varepsilon_M = \varepsilon'_M - j\varepsilon''_M$ are the complex dielectric constants of the sphere and the surrounding medium, respectively, with single and double prime standing for real and imaginary parts. Both are functions of frequency. In the quasi-static approximation, the field $\underline{E}_{\rm rms}$ may again be determined by solving Laplace's equation numerically for a different set of surface potentials representing the ac electric field amplitudes. Combination of (1)–(5) then leads to the trajectory equation:

$$\underline{u} = \underline{u}_M + k_S\underline{E}_S + k_{\rm DC}\nabla|\underline{E}_S|^2 + k_{\rm AC}\nabla|\underline{E}_{\rm rms}|^2. \tag{6}$$

Here, the coefficients $k_S, k_{\rm DC}$, and $k_{\rm AC}$ are given by

$$\begin{aligned} k_S &= q/6\pi\eta R \\ k_{\rm DC} &= (R^2\varepsilon_M/3\eta)\,{\rm Re}[f_{\rm CM}(0)] \\ k_{\rm AC} &= (R^2\varepsilon_M/3\eta)\,{\rm Re}[f_{\rm CM}(\omega)]. \end{aligned} \tag{7}$$

The presence of η in the denominator of all coefficients implies that trapping from a gas is likely to be much faster than from a liquid, although the resulting trajectories are likely to be similar. Since $\underline{u} = d\underline{r}/dt$, where $\underline{r}$ is the position vector and t is the time, we may then obtain

$$\begin{aligned} dx/dt &= u_{Mx} + k_S\underline{E}_{Sx} + k_{\rm DC}\partial|\underline{E}_S|^2/\partial x + k_{\rm AC}\partial|\underline{E}_{\rm rms}|^2/\partial x \\ dy/dt &= u_{My} + k_S\underline{E}_{Sy} + k_{\rm DC}\partial|\underline{E}_S|^2/\partial y + k_{\rm AC}\partial|\underline{E}_{\rm rms}|^2/\partial y \\ dy/dx &= u_y/u_x. \end{aligned} \tag{8}$$

Equations (8) may then be integrated numerically from given starting conditions. Clearly, if there are no fields, $dy/dx = u_{My}/u_{Mx}$ and the trajectories follow the gas streamlines. Fields then modify the trajectories. The result will depend strongly on the exact system parameters. In detail, these include nanoparticle properties (dielectric constant, radius, and charge), gas properties (viscosity and dielectric constant), and operational parameters (gas flow velocity and electric field definition). More generally, the relative significance of different effects depends mainly on the field and coefficient magnitudes. The various regimes may, therefore, be illustrated by assuming electrode potentials as either ± 1 V as required and varying the k-values.

Note that the argument above implies that the absolute values of the Clausius–Mossotti factors (and the ac frequency) are

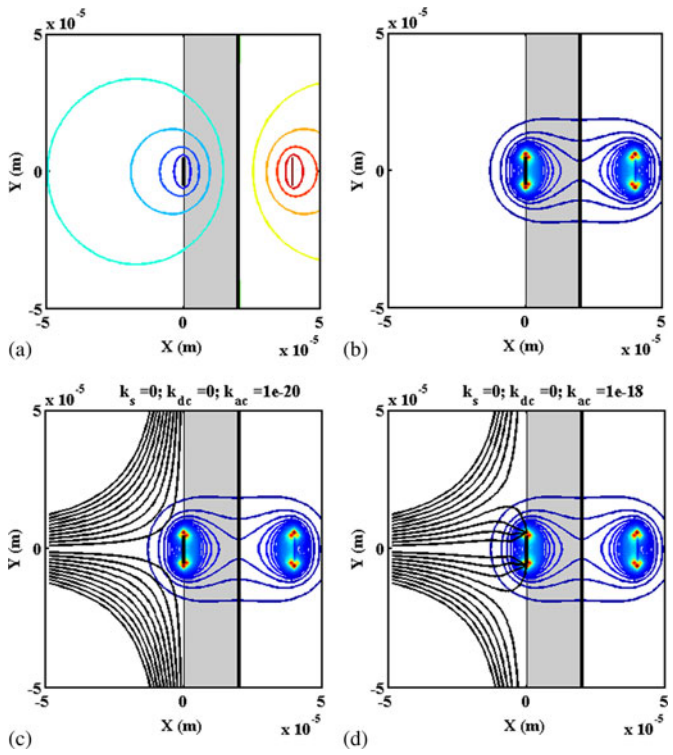

Fig. 3. (a) Equipotentials and (b) trapping potentials for ac fields; (c) and (d) Trajectories during ac DEP, for increasing values of k_{AC}.

unimportant on their own. However, in the simulations that follow, we assume positive k-values, which in turn implies positive Clausius–Mossotti factors.

IV. Numerical Results

An algorithm was written to perform the necessary calculations, and typical results are shown in Figs. 3 and 4. Here, a set of nanoparticles carried by a gas stream is assumed to impinge from the left on a trap mounted on a chargeable dielectric. We assume a microstrip trap of width 10 μm separated from a ground plane by a 20-μm-thick air-gap, and that electric fields are derived from voltages of plus or minus unity for both dc and ac potentials. Fields are calculated inside a grounded enclosure ranging from -200 to $+200$ μm in the x- and y-directions, using a 1-μm grid, but results are plotted over a smaller range from -50 to $+50$ μm.

Fig. 3(a) and (b) shows the equipotentials and normalized trapping potential due to ac voltages, respectively. Here, the substrate is shaded gray and the electrodes are indicated by bold lines. The equipotentials are clustered around the strip electrod, and also around a second "image" electrode, which is irrelevant for trapping purposes. The trapping potential has foci near each of the four electrode edges.

To simulate particle trajectories, we assume a flow velocity constant $A = 1$, leading to an integration time of around 6 s. We start by considering ac trapping during pneumatic spray, when no charges need be considered. Fig. 3(c) and (d) shows trajectories for different values of k_{AC} increasing over two orders of magnitude, superimposed on contours of normalized ac

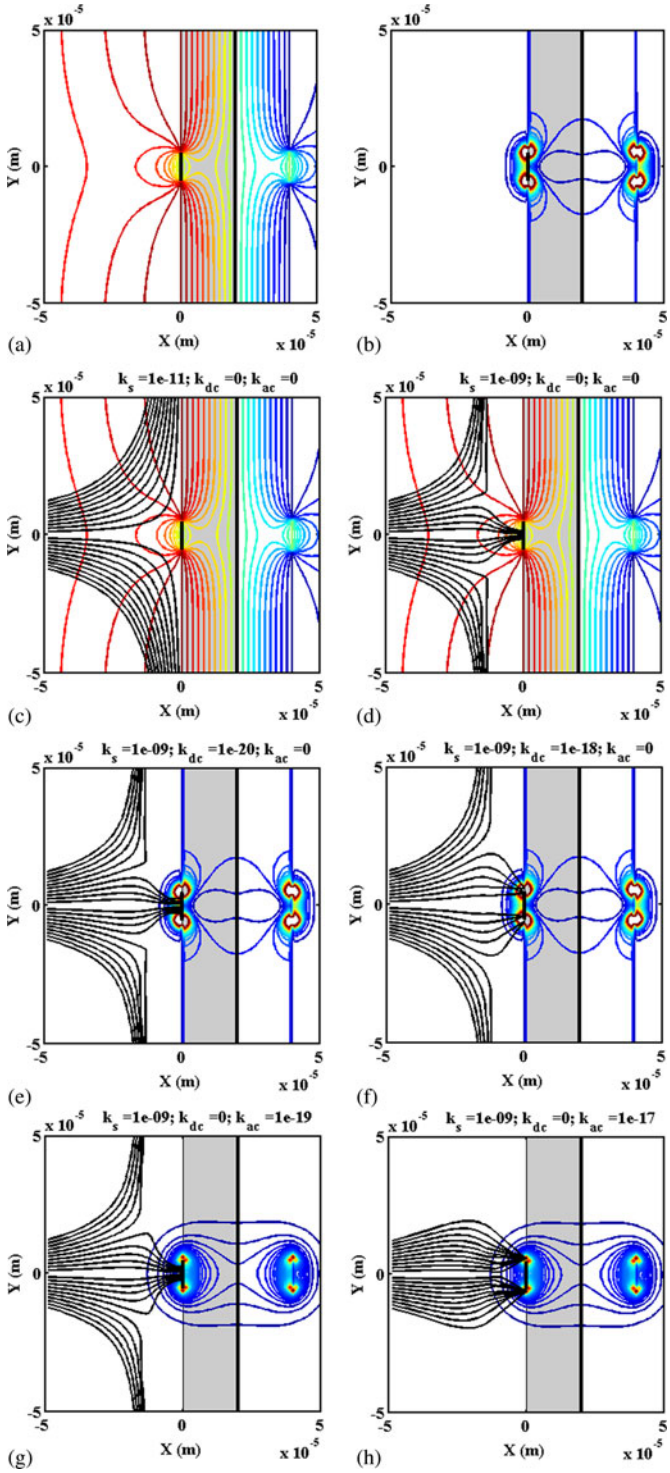

Fig. 4. (a) Equipotentials and (b) trapping potentials (RH) for dc fields; and trajectories during dc charge repulsion, for increasing values of (c) and (d) k_S, (e) and (f) k_{DC}, and (g) and (h) k_{AC}.

trapping potential. For small k_{AC}, the flow stream approaches the trapping plane and then diverges symmetrically. However, as k_{AC} rises, the trajectories increasingly divert toward the two real trapping foci, showing that the trapping force can overcome viscous drag when the ac voltage is large enough. However,

untrapped particles approach the electrode plane closely, and as a result, we would expect random decoration elsewhere.

We now consider the additional effects that may occur during electrospray. Fig. 4(a) and (b) shows the equipotentials and normalized trapping potential due to uniform dc charging of areas outside the electrode surface, respectively, assuming the electrodes themselves are grounded. Once again these are derived from the real potentials and a set of "image" potentials. The trapping potential again has four foci: two real and two virtual.

Fig. 4(c) and (d) shows particle trajectories for different values of k_S, again increasing over two orders of magnitude, superimposed on the dc equipotentials. For small k_S, the flow stream approaches the trapping plane and then diverges symmetrically. However, as k_S rises, two effects can be seen. Off-axis trajectories are repelled from the dc potential barrier created by the charged surfaces, while on-axis trajectories are forced toward the center of the trapping electrode. The first phenomenon should result in a reduction in random surface decoration, while the second phenomenon leads to charge heaping, previously observed by Kim *et al.* [25]. Similar effects are observed when the strip electrode is held at an attractive potential designed to mimic dc trapping.

Fig. 4(e) and (f) shows similar trajectories for a fixed value of k_S but different values of k_{DC}, superimposed on contours of normalized dc trapping potential. For small k_{DC}, charge repulsion and heaping occur as before. However, as k_{DC} rises, nanoparticles previously forced toward the electrode center are now trapped by dc DEP at the electrode edge. However, since k_{DC} is strictly proportional to k_S, we might expect the effect to be small. Conversely, since k_{AC} is an independent variable, we might expect much larger ac trapping effects. Fig. 4(g) and (h) shows similar trajectories for a fixed value of k_S but different values of k_{AC}, now superimposed on contours of normalized ac trapping potential. For small k_{AC}, charge repulsion and charge heaping occur as before. However, as k_{AC} rises, nanoparticles are increasingly trapped by ac DEP. This result shows that ac trapping can also ovecome the joint effects of charge repulsion and charge heaping when the voltage is large enough.

Comparable simulations were carried out for the coplanar electrode geometry of Fig. 1(a). All the phenomena of Figs. 3 and 4 were observed, namely the formation of trapping focii at the electrodes, and both dc and ac dielectrophoretic effects. Charge repulsion and heaping were also both observed in simulations of electrospray. However, because this geometry consists of a single dielectric region between two electrodes, charges are repulsed symmetrically away from the electrode gap, and charge heaping occurs just above and below the upper and lower electrode edges.

We may summarize these results as follows. Trapping is determined from a balance of the forces involved. For neutral particles, particles are either trapped or not, depending on the gas flow rate and the starting condition. Particles starting strongly off-axis in a relatively strong gas flow are not trapped, and trapping probability is increased toward the center of weaker flows. The trajectories of trapped particles end at electrode edges where the trapping foci are located. However, for charged particles, some trajectories are forced away from these foci toward the electrode centers, due to surface charge repulsion.

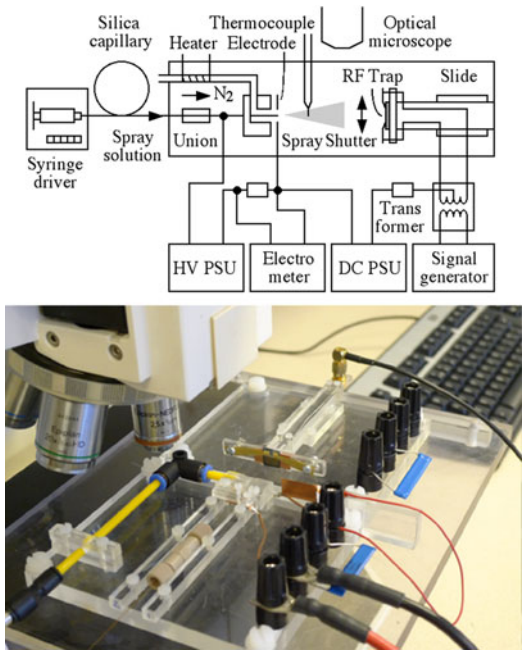

Fig. 5. Arrangement and realization of experimental rig.

V. Experimental Results

To investigate the effects previously described, a Perspex experimental rig was developed that allows fluorescent nanoparticles to be sprayed perpendicularly onto a microfabricated chip carrying patterned electrodes, as shown in Fig. 5. The setup allows both pneumatic spray and nanospray.

Liquid flow was generated using a programmable syringe pump (KD Scientific 100 series) with a glass syringe (Hamilton 250 μL), which continuously delivers spray solution at low flow rates to a nanospray capillary. A small capillary diameter is needed to reduce the voltage for electrospray. However, the ID should be large enough to avoid clogging by nanoparticles. Coated SilicaTips (New Objective) with proximal metal coating and 30-μm inner diameter were found to be suitable.

A 1-mm ID coaxial nebulizer was used to provide a continuous flow of N_2 from a gas cylinder. The gas velocity cannot be measured directly but can be controlled using the upstream gas pressure. In all experiments, it was essential to dry the spray. Otherwise, the gas stream was found to contain a significant fraction of liquid droplets. The gas was, therefore, heated using an electrical heater based on a 10-W resistor attached to a stainless steel section of the gas delivery pipe, and the downstream gas temperature measured using a thermocouple. Heater temperatures of $\approx$130 °C led to nebulizer gas temperatures of $\approx$30 °C.

For electrospray, a thin photoetched stainless steel electrode with a circular aperture (800-μm diameter) was placed at a short distance (100–150 μm) from the capillary tip. A high-voltage dc power supply (HP 6515A) generated the voltage between the tip and the counterelectrode, and a low-voltage PSU was

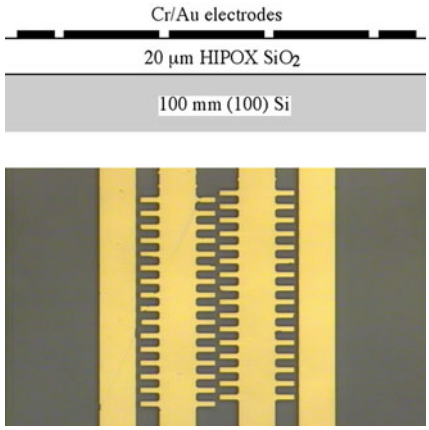

Fig. 6. Layout and realization of trapping electrodes.

used to control the dc potential of the trap. An electrometer (Keithley 6517) was used to monitor the spray, by measuring the voltage across a current-limiting resistor. The dc voltage was in the range of 1.0–1.4 kV, the solution was supplied with a flow rate of 12–15 μL/h, and the nebulizer gas flow rate was tuned to achieve a stable spray. The trapping electrodes were at a distance of 1–1.5 cm, and spraying was carried out for 2–4 min. For pneumatic spraying, the counterelectrode and the dc power supplies and monitors were simply removed, so that an aerosol was generated directly. Larger gas flow rates were required to achieve atomization, and the trapping electrodes could then be placed at a larger distance (2–4 cm) from the capillary.

The trapping system was a chip with different planar electrode configurations, as shown in Fig. 6. The fingers were connected to bus bars to connect all electrode pairs to the drive voltage. The fingers and bus bars are 20 and 50 μm wide, respectively, and the electrode gaps are 20 μm. The chip was fabricated on a $\langle 1\ 0\ 0 \rangle$ Si wafer, with a 20-μm-thick SiO_2 insulation layer and Cr/Au electrodes.

DC voltages were generated using a low-voltage PSU, and ac voltages using a signal generator (Thurlby Thandar TG1010) and a step-up transformer, reaching maximum voltages of 300 V p-p at 10 kHz. The frequency was chosen to obtain good performance from the transformer, while remaining in the frequency range for which the nanoparticles used exhibited strong DEP effects. In-plane traps were realized by connecting to opposing electrode sets. Microstrip traps were realized by connecting all surface electrodes to a common potential and connecting with silver-loaded epoxy to the Si substrate, which then provided a ground plane. However, some distortion of the ac signal was observed in this mode, presumably due to diode behavior at the silicon contact.

The nanoparticles were 50-nm diameter fluorescent nanospheres (Sigma Aldrich L0780, amine-modified polystyrene) with excitation and emission wavelengths of λ_{ex} ~360 nm and λ_{em} ~420 nm, respectively. For polystyrene in DI water, $\mathrm{Re}(f_{\mathrm{CM}})$ is approximately constant, positive and at its maximum value up to frequencies >10 kHz [21]. The nanospheres were dispersed in a solvent consisting of 75% DI water, 20% methanol, and 5% acetic acid to increase the conductivity.

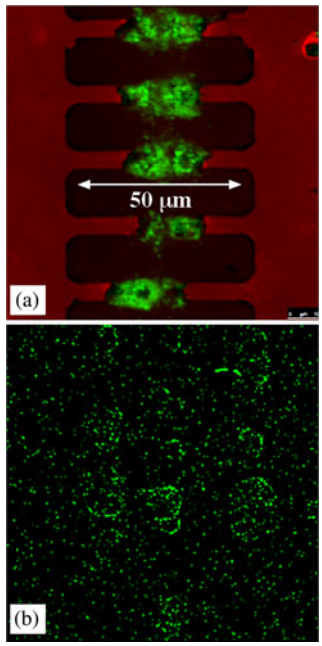

Fig. 7. Experimental results for nanospheres sprayed onto coplanar traps with an ac trapping voltage. (a) Electrospray, showing the effects of plasma discharge. (b) Pneumatic spray, showing the signs of convective self-assembly arising from liquid droplets striking the substrate.

Solution preparation involved addition of a small additional amount (<1%) of surfactant and sonication for at least 15 min. Cone-jet formation was observed using an optical microscope, and stable spraying was achieved at 0.05–0.1 vol% concentration of nanospheres. Examination of the deposited patterns was carried out with a confocal fluorescence microscope (Leica SP5) equipped with an Ar^+ laser for visible imaging and a tunable multiphoton laser (Spectra-Physics Mai Tai Ti:sapphire) for fluorescence imaging. The combination allows optical images of the electrode system and the fluorescent nanosphere patterns to be acquired separately and subsequently overlaid.

A number of experiments were carried out. Both pneumatic and electrospraying modes were used, dc and ac voltages were applied to the electrodes, and in-plane and microstrip electrodes were investigated. However, in-plane electrodes were generally damaged by a plasma discharge. Although trapping was consistently observed, deposition was mainly seen between the electrodes, rather than on the trapping foci. Fig. 7(a) shows a fluorescence microscope image highlighting this effect. Any DEP-driven nanosphere decoration generally followed the original outlines of electrodes that were subsequently eroded by sputtering. Even if discharge could be avoided, it was important to desolvate the spray thoroughly. Otherwise, gas phase trapping effects were masked by convective self-assembly, as liquid droplets dried on the target substrate. Fig. 7(b) shows the characteristic meniscal stains left by convective self-assembly.

Microstrip electrodes routinely gave more successful results, especially with careful dehydration of the spray. Fig. 8(a) shows a uniform surface decoration obtained while pneumatically spraying onto a microstrip trap without an applied voltage. This figure demonstrates the relatively uniform coating obtained

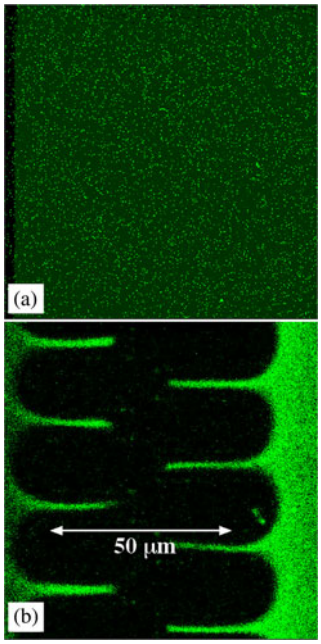

Fig. 8. Experimental results for nanospheres sprayed onto microstrip traps. (a) Pneumatic spray, no applied voltage. (b) Electrospray with dc voltage.

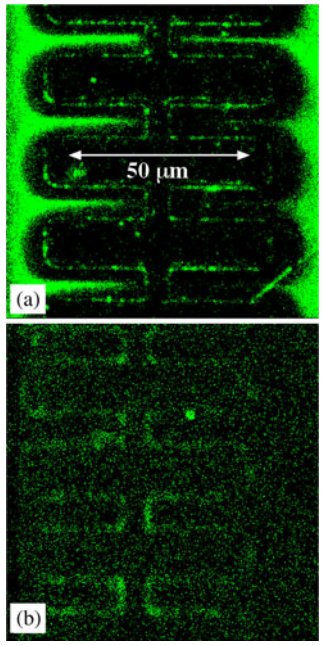

Fig. 9. Experimental results for nanospheres sprayed onto microstrip traps. (a) Electrospray with ac voltage. (b) Pneumatic spray with ac voltage.

without a trapping field and the general failure of purely pneumatic spraying to yield clean surfaces.

Fig. 8(b) shows the corresponding pattern obtained during electrospray with a simple dc attractive potential. Here, the decoration approximately follows the electrode shapes, but charge heaping has forced the nanospheres to lie within the electrode areas. There is little edge decoration, suggesting that dc dielectrophoretic effects are indeed relatively unimportant. A subsidiary effect of surface charging is to reduce contamination of the dielectric areas. The effects seen in this figure broadly correspond to the simulated results in Fig. 4(d), where charged nanoparticles are forced to the center of the electrode by the equivalent surface potential.

Fig. 9(a) shows the corresponding result obtained during electrospray with an ac trapping voltage. The results are generally similar to Fig. 8(b). However, an additional edge decoration has clearly been induced by ac DEP, and a thin nanosphere pattern can now be seen, following the electrode outline. The ac trapping effect is clearly less visible using a confocal imaging system, since large areas are no longer coated, and the nanospheres are likely to pile-up out-of-plane. The effects seen in this figure broadly correspond to the simulated results in Fig. 4(g), where charge heaping and trapping are in competition.

Finally, Fig. 9(b) shows the corresponding result achieved during pneumatic spray with an ac voltage applied. Trapping is now achieved without any charge heaping; only the electrode outline may be seen, and the main electrode areas are no longer coated. However, a uniform and random distribution of deposit is visible elsewhere. The effects seen in this figure broadly correspond to the simulated results in Fig. 3(d), where trapping is only in competition with viscous drag.

Some similar patterns were observed with coplanar electrodes. However, discharge effects generally confused the results. For example, deposits were often formed at the edges of electrodes during dielectrophoretic trapping, but any discharge-induced sputtering led to a migration of the edge and its associated pattern away from the electrode gap.

These results broadly confirm the predictions of the analytic model and demonstrate that switching between the different trapping modes may be achieved using careful control of the nanosphere charge state and the trapping potential.

VI. Conclusion

The combination of spray-based presentation of nanoparticles and electric field trapping has been shown to offer considerable flexibility for nanoscale patterning, and confocal fluorescence microscopy has been shown to provide a convenient method of visualizing gross particle distributions. Scavenging particles from a gas rather than a liquid phase has the advantage of reduced viscous forces, so that rapid coating may be achieved, the spray may be directed toward the trapping region, and the deposit is inherently dry. All aspects offer improvements in trapping performance.

Experimental results confirm an independent-particle model that includes the effect of viscous drag, dc and ac potentials, and their spatial variations. Both show that different patterning effects can be achieved using combinations of spraying modes and trapping fields. Trapping can be carried out from pneumatically generated spray and electrospray. The former has the potential for cleaner patterns, since it forms a deposit mainly in designated trapping regions. However, the latter is likely to generate a more uniform dispersion. DC fields can be used to trap charged nanoparticles. In this case, patterns generally follow the electrode shapes, but repulsive forces from adjacent surface charges lead to patterns smaller than electrode dimensions. AC

DEP can trap both charged and uncharged nanoparticles, and has the potential for higher resolution since the deposits follow electrode edges. Future work in this area will, therefore, explore high-resolution patterning on separate thin-film substrates. Although not explored here, a key advantage of DEP trapping is its ability to orient nonspherical particles, which should allow the deposition of aligned nanostructures. A further advantage is its selectivity, which should allow the implementation of sorting functions, and open applications in (for example) DEP-enhanced mass sensors [30].

ACKNOWLEDGMENT

The authors are extremely grateful to P. Jones for fabrication of the experimental setup, to Dr. K. Choonee for fabrication of the microelectrode array, and to Dr. M. Spitaler for support in fluorescence imaging.

REFERENCES

[1] T. Fukuda, F. Arai, and L. Dong, "Assembly of nanodevices with carbon nanotubes through nanorobotic manipulations," *Proc. IEEE*, vol. 91, no. 11, pp. 1803–1818, Nov. 2003.

[2] Y. Wang, D. Maspoch, S. Zou, G. C. Schatz, R. E. Smalley, and C. A. Mirkin, "Controlling the shape, orientation, and linkage of carbon nanotube features with nano affinity templates," *PNAS*, vol. 103, pp. 2026–2031, 2006.

[3] H. Xin and A. T. Woolley, "Directional orientation of carbon nanotubes on surfaces using a gas flow cell," *Nano Letts.*, vol. 4, pp. 1481–1484, 2004.

[4] P. A. Kralchevsky, N. D. Denkov, V. N. Paunov, O. D. Velev, I. B. Ivanov, H. Yoshimura, and K. Nagayama, "Formation of 2-dimensional colloid crystals in liquid-films under the action of capillary forces," *J. Phys. Cond. Matt*, vol. 6, pp. A395–A402, 1994.

[5] J. A. Liddle, Y. Cui, and P. Alivisatos, "Lithographically directed self-assembly of nanostructures," *J. Vac. Sci. Technol. B*, vol. 22, pp. 3409–3414, 2004.

[6] S. Tan, H. A. Lopez, C. W. Cai, and Y. Zhang, "Optical trapping of single-walled carbon nanotubes," *Nano Letts.*, vol. 4, pp. 1415–1419, 2004.

[7] T. Yu, F.-C. Cheung, and C.-H. Sow, "The manipulation and assembly of CuO nanorods with line optical tweezers," *Nanotechnology*, vol. 15, pp. 1732–1736, 2004.

[8] M. Tanase, D. M. Silevitch, A. Hultgren, L. A. Bauer, P. C. Searson, G. J. Meyer, and D. H. Reich, "Magnetic trapping and self-assembly of multicomponent nanowires," *J. Appl. Phys.*, vol. 91, pp. 8459–8551, 2002.

[9] N. Naujoks and A. Stemmer, "Micro- and nanoxerography in liquids – controlling pattern definition," *Microelectr. Eng.*, vol. 78–79, pp. 331–337, 2005.

[10] P. Mesquida and A. Stemmer, "Maskless nanofabrication using the electrostatic attachment of gold particles to electrically patterned surfaces," *Microelectr. Eng.*, vol. 61/62, pp. 671–674, 2002.

[11] H. O. Jacobs, S. A. Campbell, and M. G. Steward, "Approaching nanoxerography: The use of electrostatic forces to position nanoparticles with 100 nm scale resolution," *Adv. Mater.*, vol. 14, pp. 1553–1557, 2002.

[12] H. A. Pohl, *Dielectrophoresis*. Cambridge, U.K.: Cambridge Univ. Press, 1978.

[13] P. A. Smith, C. D. Nordquist, T. N. Jackson, T. S. Mayer, B. R. Martin, J. Mbindyo, and T. E. Mallouk, "Electric-field assisted assembly and alignment of metallic nanowires," *Appl. Phys. Lett.*, vol. 77, pp. 1399–1401, 2000.

[14] K. D. Hermanson, S. O. Lumsdon, J. P. Williams, E. W. Kaler, and O. D. Velev, "Dielectrophoretic assembly of electrically functional microwires from nanoparticle suspensions," *Science*, vol. 294, pp. 1082–1086, 2001.

[15] R. Krupke, F. Hennrich, M. M. Kappes, and H. v. Löhneysen, "Surface conductance induced dielectrophoresis of semiconducting single-walled carbon nanotubes," *Nano Lett.*, vol. 4, pp. 1395–1399, 2004.

[16] E. B. Cummings and A. K. Singh, "Dielectrophoresis in microchips containing arrays of insulating posts: Theoretical and experimental results," *Anal. Chem.*, vol. 75, pp. 4724–4731, 2003.

[17] D. C. Chen, H. Du, and C. Y. Tay, "Rapid concentration of nanoparticles with dc dielectrophoresis in focused electric fields," *Nanoscale Res. Lett.*, vol. 5, pp. 55–60, 2010.

[18] S. O. Lumsdon, E. W. Kaler, and O. D. Velev, "Two dimensional crystallization of microspheres by a coplanar ac electric field," *Langmuir*, vol. 20, pp. 2108–2116, 2004.

[19] Y. J. Yuan, M. K. Andrews, and B. K. Marlow, "Chaining and dendrite formation of gold particles," *Appl. Phys. Lett.*, vol. 85, pp. 130–132, 2004.

[20] N. G. Green and H. Morgan, "Dielectrophoretic separation of nanoparticles," *J. Phys. D. Appl. Phys.*, vol. 30, pp. L41–L84, 1997.

[21] C. Zhang, K. Khooshmanesh, F. J. Tovar-Lopez, A. Mitchell, W. Wlodarski, and K. Klantar-Zadeh, "Dielectrophoretic separation of carbon nanotubes and polystyrene microparticles," *Microfluid. Nanofluid.*, vol. 7, pp. 633–645, 2009.

[22] O. V. Salata, "Tools of nanotechnology: Electrospray," *Curr. Nanosci.*, vol. 1, pp. 25–33, 2005.

[23] A. Jaworek and A. T. Sobczyk, "Electrospraying route to nanotechnology: An overview," *J. Electrostat.*, vol. 66, pp. 197–219, 2008.

[24] S. Khan and Y. H. Doh, "Direct patterning and electrospray deposition through EHD for fabrication of printed thin film transistors," *Curr. Appl. Phys.*, vol. 11, pp. S217–S279, 2011.

[25] J.-W. Kim, Y. Yamagata, B. J. Kim, and T. Higuchi, "Direct and dry micro-patterning of nano-particles by electrospray deposition through a micro-stencil mask," *J. Micromech. Microeng.*, vol. 19, p. 025021, 2009.

[26] A. M. Welle and H. O. Jacobs, "Printing of organic and inorganic nanomaterials using electrospray ionization and coulomb-force directed assembly," *Appl. Phys. Lett.*, vol. 87, pp. 263119-1–263119-3, 2005.

[27] M. Cloupeau and B. Prunet-Foch, "Electrostatic spraying of liquids in cone-jet mode," *J. Electrostat.*, vol. 22, pp. 135–159, 1989.

[28] D. C. Gale and R. D. Smith, "Small volume and low flow-rate electrospray ionization mass spectrometry of aqueous samples," *Rapid Commun. Mass Spectrom.*, vol. 7, pp. 1017–1021, 1993.

[29] M. Busman and J. Sunner, "Simulation method for potential and charge distributions in space charge dominated ion sources," *Int. J. Mass Spectrom. Ion Proc.*, vol. 108, pp. 165–178, 1991.

[30] H. O. Fatoyinbo, K. F. Hoettges, S. M. Reddy, and M. P. Hughes, "An integrated dielectrophoretic quartz crystal microbalance (DEP-QCM) device for rapid biosensing applications," *Biosens. Bioelectron.*, vol. 23, pp. 225–232, 2007.

Marcel Tichem received the M.Sc. degree in 1991 and the Ph.D. degree in 1997, both from Delft University of Technology, Delft, The Netherlands.

He is currently an Associate Professor at the Micro and Nano Engineering Laboratory, Faculty of Mechanical, Maritime and Materials Engineering, Delft University of Technology. His research program focuses on microassembly and heterogeneous integration. His specific research interests include photonic integration and submicrometer alignment using passive and active microfabricated structures, self-assembly at microscale, foil-based systems, and nanoscale patterning. He coordinates the EU FP7 funded collaborative project Chip2Foil. In 2011, he worked at the Optical and Semiconductor Devices Group in the Department of Electrical and Electronic Engineering, Imperial College London, London, U.K., on the basis of an EU FP7 Marie Curie IEF training grant to explore volume manufacturing methods for realizing discrete patterns of nanoscale objects.

Richard R. A. Syms (SM'02) received the B.A. and D.Phil. degrees in engineering science, Oxford University, Oxford, U.K., in 1979 and 1982, respectively.

He has been the Head of the Optical and Semiconductor Devices Group in the Department of Electrical and Electronic Engineering, Imperial College London, London, U.K., since 1992, and a Professor of Microsystems Technology since 1996. He currently lectures on guided wave optics and electromagnetic theory. He has contributed to more than 150 journal papers, 80 conference papers, and two books on holography, integrated optics, metamaterials, and microengineering. Most recently, he has been developing 3-D self-assembling microstructures. miniature quadrupole mass spectrometers, optical microelectromechanical systems (MEMS) such variable attenuators and tunable lasers, and RF probes for magnetic resonance imaging. He has consulted widely on guided wave optics and MEMS, and cofounded the MEMS spin-out company Microsaic Systems in 2001.

He is currently an Associate Editor for the *Journal of Microelectromechanical Systems* and for *Metamaterials*. He has served on many MEMS review panels, including for the EPSRC Microsystems Technology Integration Program, and the German, Canadian, and Singaporean MEMS programs. He is a Fellow of the Royal Academy of Engineering, the Institute of Physics, and the Institute of Electrical Engineers.